Estimation of electron dynamics using ensemble Kalman filtering

IEPC-2025-674

Presented at the 39th International Electric Propulsion Conference
Imperial College London, London, UK
September 14-19, 2025

Kentaro Hara[1]
Stanford University, Stanford, California 94305, USA

Anubhav Dwivedi[2]
University of Minnesota, Minnesota 55455, USA

In this paper, we summarize our ongoing efforts toward estimating electron dynamics using variations of Kalman filters. First, we have developed an ensemble Kalman filter (EnKF) that is coupled to a 0D collisional radiative model. Using optical emission spectroscopy data, we were able to estimate the non-Maxwellian electron energy distribution functions at various gas pressures in a capacitvely coupled plasma source. Second, we propose a 1D test case of an advection-reaction system, which is similar to the discharge plasma in Hall effect thrusters. Using an extended Kalman filter (EKF) for discretized partial differential equations, we have robustly estimated the spatio-temporal profile of the electron temperature required for a breathing mode oscillation.

I. Introduction

Electron dynamics plays a critical role in partially ionized plasmas for electric propulsion applications. Despite its importance, the physical processes in such plasmas are complex, making it difficult to understand and let alone predict electron dynamics. While high-fidelity physics-based models are required, data assimilation techniques that combine predictions from the model and measurement data can be useful in understanding the spatio-temporal profiles of the electron properties that are difficult to measure or model.

Physics-based models, such as kinetic, fluid, and hybrid models, have been developed over the past three decades. Kinetic models are mainly particle based, including particle-in-cell (PIC), Monte Carlo collision (MCC), and direct simulation Monte Carlo (DSMC). Additionally, grid-based direct kinetic (DK) methods have been used as an alternative kinetic approach. The fluid models within the HET community have traditionally relied on the drift-diffusion (DD) approximation under the assumptions of a quasineutral plasma. Recently, there have been development of fluid moment approaches, e.g., 5-moment, 10-moment, and 14-moment models, to improve upon the fidelity of fluid models. Hybrid modelling is also a common method, where ions are modelled using a particle-based kinetic method and electrons are treated as fluid.

However, regardless of the chosen model, description of the collisional and multiscale processes at play needs to be provided. For instance, the rate and transport coefficients depend on the electron energy distribution function (EEDF), while the anomalous electron transport might be driven by near-wall conductivity or plasma waves triggered by kinetic instabilities, which require high-fidelity, high-resolution kinetic models. Furthermore, plasma-wall interactions may require detailed knowledge of secondary electron emission, sputtering, and related wall effects. These properties are often estimated empirically through experiments, introducing significant uncertainties in the cross sections and the associated wall interaction modelling.

In this paper, we introduce the concepts of the data assimilation techniques. First, we present the ensemble Kalman filter (EnKF) of a 0D collisional radiative model (CRM) that uses optical emission spectroscopy (OES) data. The EEDF is parameterized and estimated using the EnKF-CRM with OES data from literature. The estimated EEDF is compared with the results obtained from a high-fidelity model by Donko et al. [1], i.e., a 1D diffusion reaction radiative

[1]Assistant Professor, Aeronautics and Astronautics, kenhara@stanford.edu
[2]Research Associate, Aerospace Engineering and Mechanics, dwive016@umn.edu

(DRR) model is coupled with a 0D Monte Carlo collision (MCC) model. Second, we discuss state and parameter estimation using an extended Kalman filter (EKF) for a set of 1D advection-reaction PDEs. Here, the model is similar to a predator-prey model but contains the advection of the predator (ions) and prey (neutral atoms), which make the equations hyperbolic. We use spatio-temporal profile of ion bulk velocities obtained from laser induced fluorescence (LIF) [2] and discharge current oscillation to estimate the spatio-temporal dynamics of electron temperature. So far, we have used EKF for this test case, but we are actively working on developing an EnKF framework. We will discuss some observations.

II. State and parameter estimation using Kalman filtering

A. 0D ODE

A state variable of a system can be defined as the information that can be updated by a set of governing equations. For instance, density, momentum, and energy in a fluid equation are state variables. However, if one has shear stress or heat flux, viscosity and thermal conductivity can be considered parameters of the system. If the state variables are $\mathbf{u}(t)$ and the parameters are $\mathbf{p}(t)$, then one can consider an augmented state vector, $\mathbf{s} = [\mathbf{u}, \mathbf{p}]^\top$.

The key idea of Kalman filtering is that a model (i.e., mathematical model) and data (i.e., measurement obtained from experiments) are combined to estimate, infer, and control the system. The underlying philosophy relies on the fact that any state variable and parameter is *unknown*, thus can be described by a probability density function (PDF). Similar to kinetic methods in gas and plasma dynamics, the main question of the propagation of PDF is whether the PDF is a Gaussian or non-Gaussian. The process of state and parameter estimation is explained in Fig. 1. First, with a given model, the initial PDF is propagated in time. The PDFs can be characterized, similar to kinetic methods, using the moments of the PDF, e.g., the mean $\hat{\mathbf{s}} = E(\mathbf{s})$ and the covariance $P = E[(\mathbf{s} - \hat{\mathbf{s}})(\mathbf{s} - \hat{\mathbf{s}})^\top]$, where E is the expectation. For a state vector of size N, the mean is also a state vector of size N and the covariance becomes a $N \times N$ matrix. Second, when the measurement becomes available at discrete times, e.g., t_1, t_2, ..., the PDF of estimated state variables and parameters gets updated. The assimilation process can be considered a Bayesian type approach where the prior PDF (from the model) is updated to a posterior PDF (based on measurement). It is important to note that the measurement data also have their own uncertainties.

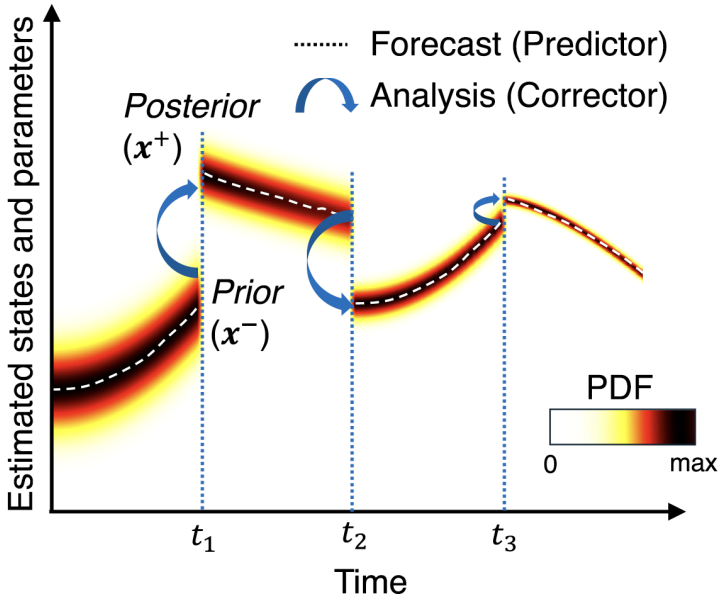

Fig. 1 Estimation of state variables and parameters based on filtering. The colorbar shows the probability density function (PDF) of the estimated state variables and parameters. This can be directly applied to a 0D ordinary differential equation (ODE). Reproduced from Ref. 3.

For Kalman filtering, the model is typically generalized as

$$\frac{d\mathbf{u}}{dt} = \mathbf{f}(\mathbf{u}, \mathbf{p}) + \mathbf{w}_u, \tag{1}$$

where $\mathbf{f}$ is the dynamical model function and the parameters are defined as the variables that are not updated by the model and $\mathbf{w}_u$ is the process noise for a state variable $\mathbf{u}$. For a parameter, one can write $d\mathbf{p}/dt = \mathbf{w}_p$, where $\mathbf{w}_p$ is the process noise associated with the parameter. The measurement data are typically considered as

$$\mathbf{y} = \mathbf{h}(\mathbf{u}) + \mathbf{v}, \tag{2}$$

where $\mathbf{h}$ is the measurement function and $\mathbf{v}$ is the measurement noise.

1. Extended Kalman filter

First, initial estimates for the augmented state vector $\hat{\mathbf{s}}_0 = \hat{\mathbf{s}}(t = 0)$ and the error covariance matrix $P_0 := P(t = 0)$ are chosen. Next, for each time step that we obtain the data, we perform the following sub-steps until all time samples have been utilized.

We predict the state variables that includes parameters, $\hat{\mathbf{s}}$, and their covariances, P, until the time when measurement data set arrives. Here, superscripts + and − denote the estimates after and before the measurement update. The physics-based model is employed between t^+_{k-1} and t^-_k, where k denotes the time step at which measurements are obtained. The mean estimate is updated as,

$$\frac{d\hat{\mathbf{s}}}{dt} = \begin{bmatrix} \mathbf{f}(\hat{\mathbf{s}}, t) \\ 0 \end{bmatrix}. \tag{3}$$

The transport equation for the covariance matrix can be written as

$$\frac{dP}{dt} = LP + PL^\intercal + Q(t), \tag{4}$$

where L is the Jacobian matrix of $\mathbf{f}$ evaluated at $\hat{\mathbf{s}}$ defined as

$$L := \frac{\partial}{\partial \mathbf{s}} \begin{bmatrix} \mathbf{f}(\mathbf{s}) \\ 0 \end{bmatrix}_{\mathbf{s}=\hat{\mathbf{s}}}. \tag{5}$$

and $Q(t)$ is the process noise covariance matrix.

The state vector and covariance estimates are updated when a measurement is acquired, i.e., at k-th time step as

$$\begin{aligned} \hat{\mathbf{s}}^+_k &= \hat{\mathbf{s}}^-_k + K_k[\mathbf{y}_k - \mathbf{h}(\hat{\mathbf{s}}^-_k)], \\ P^+_k &= (I - K_k H_k)P^-_k, \end{aligned} \tag{6}$$

where $\mathbf{y}$ is the measurement data, $h(\mathbf{s})$ is the measurement function, i.e., how the measurement data can be described by the state variables, $H_k := \frac{\partial}{\partial \mathbf{s}} h(s)\big|_{\mathbf{s}=\hat{\mathbf{s}}^-_k}$ is the Jacobian of the measurement function, I is the identity matrix,

$$K_k = P^-_k H^\intercal_k (H_k P^-_k H^\intercal_k + R_k)^{-1} \tag{7}$$

is the Kalman gain, and R is the measurement noise covariance matrix.

2. Ensemble Kalman filter

With ensemble Kalman filter (EnKF), the propagation of the PDFs is performed by accounting for different *incidents*, which is similar to a particle method. The initial PDF is represented by S incidents generating an ensemble. Each member of the ensemble is evolved based on the physics-based model:

$$\dot{\mathbf{s}}^{(j)}(t) = \mathbf{f}\left(\mathbf{s}^{(j)}, t\right), \tag{8}$$

where $j = 1, 2, \cdots, S$ refers to the j-th ensemble member. For instance, if we consider that the initial bulk velocity is characterized by a Gaussian distribution with a mean value of 200 m/s and a standard deviation of 10 m/s, the initial

members are sampled to represent that given PDF. The $j = 1$ element could be 195 m/s, while the next element could be 202 m/s. Based on the initial conditions, the physics-based model is used to update the state variable. It is common to not consider a process noise for the EnKF and it is to be noted that the EnKF can be considered high-fidelity than EKF because before the data assimilation process, the prior PDFs do not have to be a Gaussian distribution. In fact, the non-Gaussian nature during the model update can be captured. With the prior PDFs, the mean and covariance matrix are calculated as

$$\hat{\mathbf{s}} = \frac{1}{S}\sum_{j=1}^{S} \mathbf{s}^{(j)}, \tag{9}$$

$$P = \frac{1}{S}\sum_{j=1}^{S} [(\mathbf{s} - \hat{\mathbf{s}})(\mathbf{s} - \hat{\mathbf{s}})^{\mathsf{T}}] \tag{10}$$

For the assimilation phase, the mean value and covariance calculated from the model prediction, i.e., the prior PDFs, are calculated according to Eqs. (9) and (10), from which the Kalman gain is calculated according to Eq. (7). In EnKF, the j-th element of the ensemble is updated as

$$\mathbf{s}_k^{+(j)} = \mathbf{s}_k^{-(j)} + K_k \left[\mathbf{y}_k - \frac{\mathbf{h}\left(\mathbf{s}_k^{-(j)}\right) + \mathbf{h}(\hat{\mathbf{s}}_k^{-})}{2} \right]. \tag{11}$$

B. 1D PDE

For PDEs, we will consider that the state variables and parameters are functions of space and time. Figure 2 shows the state and parameter estimation of 1D PDEs. The state variables at a given location are updated by considering their gradients (e.g., advection and diffusion) and volumetric source terms based on the physics-based model, which can be hyperbolic, parabolic, elliptic, and reactive. When sparse measurement data are available, the PDFs of state variables and parameters are updated through the Kalman filtering.

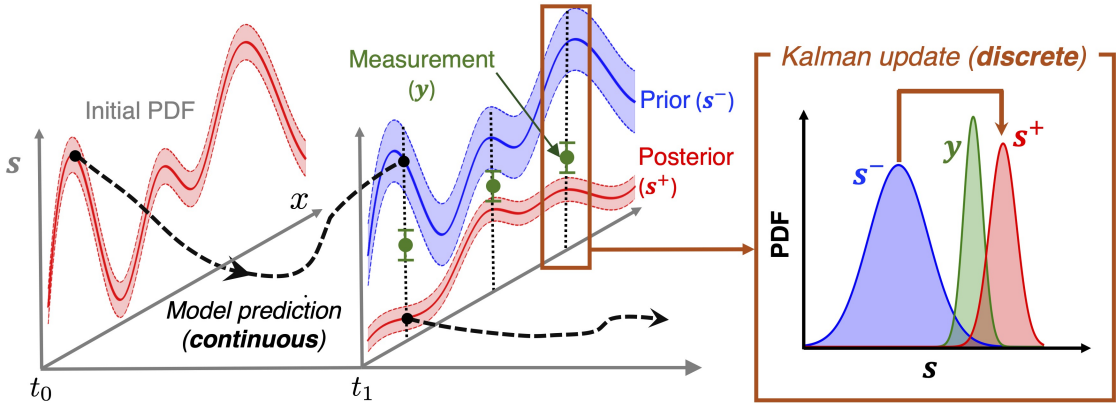

Fig. 2 Given an initial condition for the PDF of estimated state variables and parameters as a function of position, x. The model prediction updates the estimation, followed by an assimilation due to measurements that can be spatially sparse. Reproduced from Ref. 4.

To numerical solve the PDEs, the state variables and parameters are discretized first in space. Hence, the augmented

state vector can be written for the number of state variables (ν) and parameters (ρ) for n cells:

$$\mathbf{s} = \begin{bmatrix} \mathbf{u} \\ \mathbf{p} \end{bmatrix} = \begin{bmatrix} u_1(\mathbf{x}_1, t) \\ \vdots \\ u_1(\mathbf{x}_n, t) \\ \vdots \\ u_\nu(\mathbf{x}_1, t) \\ \vdots \\ u_\nu(\mathbf{x}_n, t) \\ p_1(\mathbf{x}_1, t) \\ \vdots \\ p_1(\mathbf{x}_n, t) \\ \vdots \\ p_\rho(\mathbf{x}_1, t) \\ \vdots \\ p_\rho(\mathbf{x}_n, t) \end{bmatrix} \begin{matrix} \left.\vphantom{\begin{matrix} a \\ b \\ c \\ d \end{matrix}}\right\} \text{state } \mathbf{u}_1 \\ \\ \left.\vphantom{\begin{matrix} a \\ b \\ c \\ d \end{matrix}}\right\} \text{state } \mathbf{u}_\nu \\ \\ \left.\vphantom{\begin{matrix} a \\ b \\ c \\ d \end{matrix}}\right\} \text{parameter } \mathbf{p}_1 \\ \\ \left.\vphantom{\begin{matrix} a \\ b \\ c \\ d \end{matrix}}\right\} \text{parameter } \mathbf{p}_\rho \end{matrix} , \tag{12}$$

where $\mathbf{x}_k$ is the discretized locations ($k = 1, 2, \cdots, n$).

Here, we assume that the uncertainties are uncorrelated in time. The process noise covariance can be written as

$$\mathbb{E}\left[\mathbf{w}_{s_i}(t)\mathbf{w}_{s_j}(\tau)\right] = Q^{s_i s_j}(t)\delta(\tau - t)\delta_{ij}, \tag{13}$$

where $\delta(t)$ is the Dirac delta function and δ_{ij} is the Kronecker delta function. A similar form of the noise statistics is assumed for noise sources for the parameters. The structure of the process noise covariance matrix is described in Fig. 3. This matrix illustrates the correlation of different uncertainties on different parameters and state variables on different cells centers. For instance, if we consider $Q^{u_2 u_9}_{x_3 x_7}$, this describes the process noise between the state u_2 at x_3 position and the state u_9 at x_7 position. Up to this point, it is up to the user how to design this process noise covariance matrix.

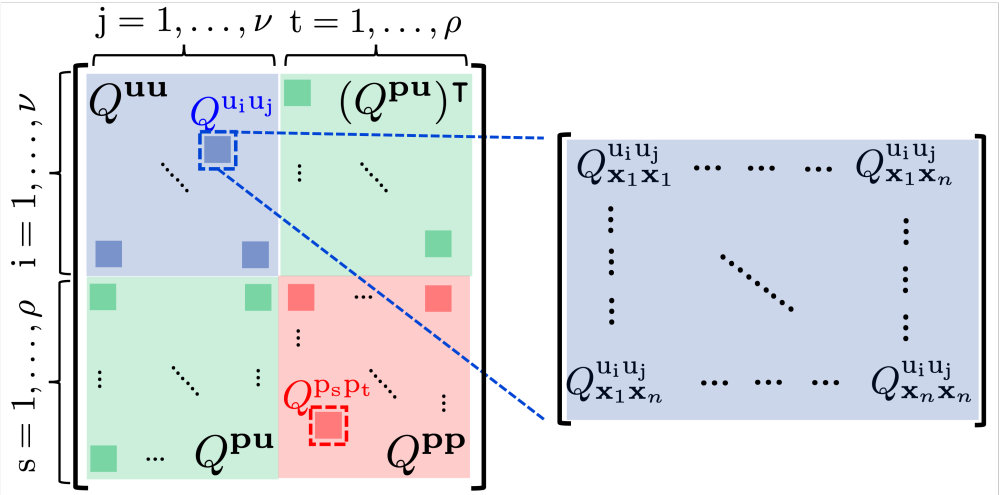

Fig. 3 The structure of the process noise covariance matrix for a PDE problem.

Furthermore, we assume that there is a spatial correlation between different locations associated with the same states and parameters to capture the influence of coupled spatial dependence of uncertainties, which is illustrated in Fig. 4. We accomplish this by parameterizing the covariance matrix in terms of a variance and a correlation matrix, i.e. $Q^{s_k s_k}(t) = \sigma_k^2(t) C^{s_k}$, where σ_i is the standard deviation and C^{s_k} is a $n \times n$ matrix that is normalized based on the state variable s_k between discrete cells. Thus, in Fig. 4, the C matrix is illustrated as $C_{x_i x_j}$ for $i = 1, \cdots, n$ and $j = 1, \cdots, n$.

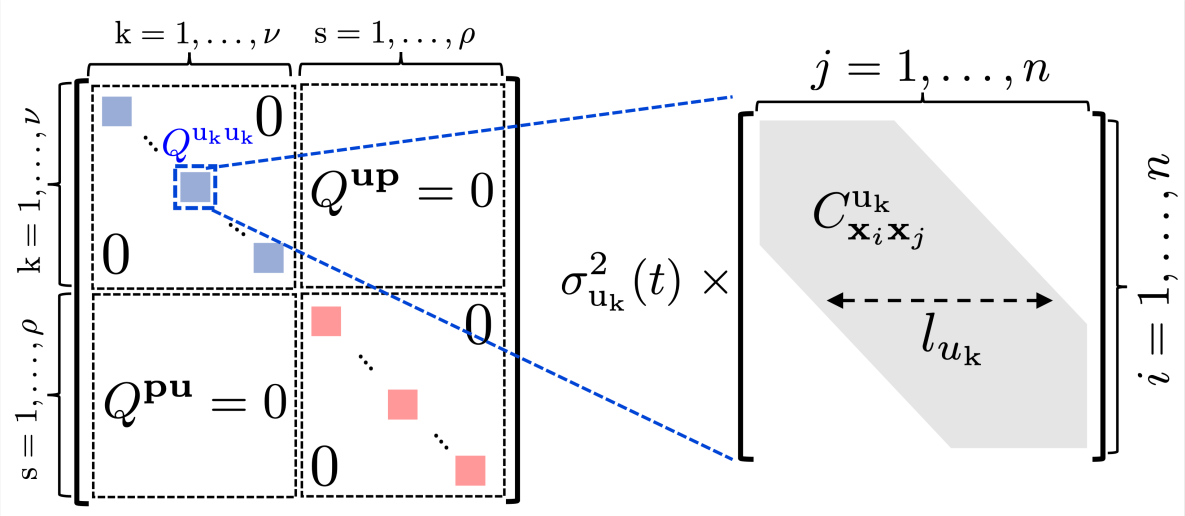

Fig. 4 Spatial correlation within process noise covariance matrix.

While a variety of correlation matrices can be used, in the present work, we adopt a Gaussian spatial correlation profile leading to

$$C^{s_k s_k}_{\mathbf{x}_m \mathbf{x}_n} = \exp\left(-\frac{|\mathbf{x}_i - \mathbf{x}_j|^2}{l^2_{s_k}}\right), \tag{14}$$

where l_{s_k} is a scalar correlation length. Such a parameterization of the spatial covariance has been shown to be successful in carrying out state estimation in neutral laminar fluids transitioning to a turbulent state [**? ?**]. In the present work, we demonstrate the utility of this variance correlation length parameterization of model uncertainty in simultaneous state and parameter estimation in nonlinear hyperbolic PDEs encountered in plasma-based applications.

Similar to the process noise, we assume that the measurement noise is uncorrelated in time but correlated in space:

$$\mathbb{E}\left[\mathbf{v}(t)\mathbf{v}^{\mathsf{T}}(\tau)\right] = R(t)\delta(t-\tau), \tag{15}$$

where $R(t)$ has block structure similar to that for covariance $Q(t)$. Accordingly, the measurement noise covariance $R(t)$ for some measurement data set $\mathbf{y}$ is given by

$$R(t) = [\sigma_y(t)]^2 \exp\left(-\frac{|\mathbf{x}_{i'} - \mathbf{x}_{j'}|^2}{l^2_y}\right), \tag{16}$$

where $\sigma_y(t)$ and l_y denote the standard deviation and correlation length, respectively, and $i' = 1, \ldots, m$ and $j' = 1, \ldots, m$. The size of the R matrix is $m \times m$ for a measurement vector of $\mathbf{y}$ that has a size of $m \times 1$.

III. Examples of recent progress on data assimilation for plasma and electric propulsion applications

A. EnKF+CRM with OES data

For an electronic excitation from energy level i to energy level j, the corresponding reaction rate coefficient can be written as,

$$k_{i\to j} = \sqrt{\frac{2}{m_e}} \int_{\varepsilon_{ij}}^{\infty} \sigma_{ij}(\varepsilon)\varepsilon^{1/2} f_e(\varepsilon)\mathrm{d}\varepsilon, \tag{17}$$

where m_e denotes the electron mass, σ_{ij} represents the collision cross section, $f_e(\varepsilon)$ determines the electron energy distribution function (EEDF), ε_{ij} is the activation energy of the said reaction, and ε is the electron kinetic energy.

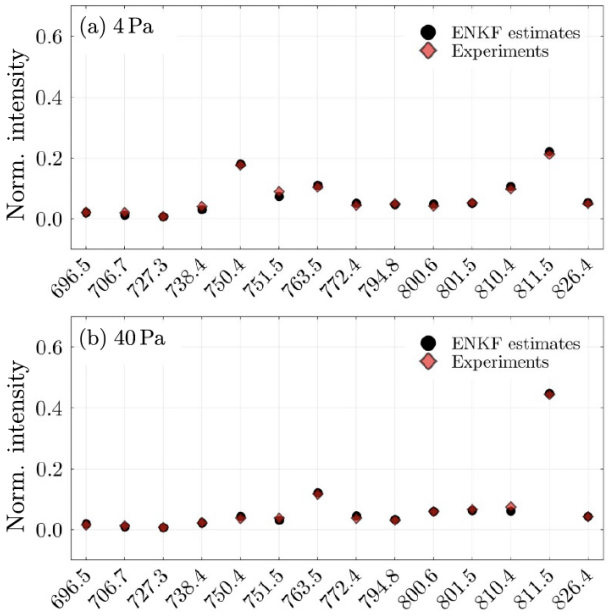

Fig. 5 Normalized optical emission intensities at selected wavelengths that are used as measurement data (taken from experiments of [1]) in the EnKF (y), compared with the calculated emission intensities. Reproduced from Ref. 4.

While the collision cross sections are often determined through detailed quantum mechanical calculations and are well documented for noble gases; the EEDF is typically a priori unknown and depends on specific discharge conditions. Furthermore, in LTPs, the EEDFs are typically non-Maxwellian distributions, often requiring computationally intensive numerical approaches (e.g., PIC/MCC) for its determination.

A widely used functional form of EEDFs in LTPs is the two-parameter (α, T_{eff}) function [5–7]:

$$f_e(\varepsilon; \alpha, T_{\text{eff}}) = c_1' T_{\text{eff}}^{-3/2} \sqrt{\varepsilon} \exp\left[-c_2' \left(\varepsilon/T_{\text{eff}}\right)^{\alpha}\right], \tag{18}$$

where

$$\begin{aligned} c_1' &= \alpha \left(\frac{2}{3}\right)^{3/2} \frac{[\Gamma(5/2\alpha)]^{3/2}}{[\Gamma(3/2\alpha)]^{5/2}}, \\ c_2' &= \left(\frac{2}{3}\right)^{\alpha} \left[\frac{\Gamma(5/2\alpha)}{\Gamma(3/2\alpha)}\right]^{\alpha}, \end{aligned} \tag{19}$$

with $\Gamma(.)$ being the Gamma function, α is a parameter that characterizes the shape of the EEDF, and T_{eff} is the effective electron temperature. The Maxwell-Boltzmann distribution corresponds to the case of $\alpha = 1$ with $c_1' = 2\pi^{-1/2}$ and $c_2' = 1$. Likewise, a Druyvesteyn distribution corresponds to the case of $\alpha = 2$ with $c_1' = 0.5652$ and $c_2' = 0.2432$. Note that T_{eff} corresponds to an effective temperature $T_{\text{eff}} = (2/3)\langle\varepsilon\rangle$, where $\langle\varepsilon\rangle$ is the electron mean energy, $\langle\varepsilon\rangle = \int_0^{\infty} \varepsilon f_e(\varepsilon) \mathrm{d}\varepsilon$. Using the parameterization of Eq. (18), we can rewrite the reaction rate coefficient in Eq. (17) as,

$$k_{i\to j}(\alpha, T_{\text{eff}}) = \sqrt{\frac{2}{m_e}} \int_{\varepsilon_{ij}}^{\infty} \sigma_{ij}(\varepsilon) \varepsilon^{1/2} f_e(\varepsilon; \alpha, T_{\text{eff}}) \mathrm{d}\varepsilon. \tag{20}$$

Figure 5 shows the normalized optical emission intensities at selected wavelengths that are used as measurement data within the EnKF. The data are taken from experiments of Ref. 1 and the measurement functions obtained from the state estimates are compared. A good agreement between the measurement data and the estimated state variables is obtained for a wide range of gas pressures, indicating that the data assimilation is performed sufficiently taking into account the measurement data and with sufficient fidelity of the physics-based model.

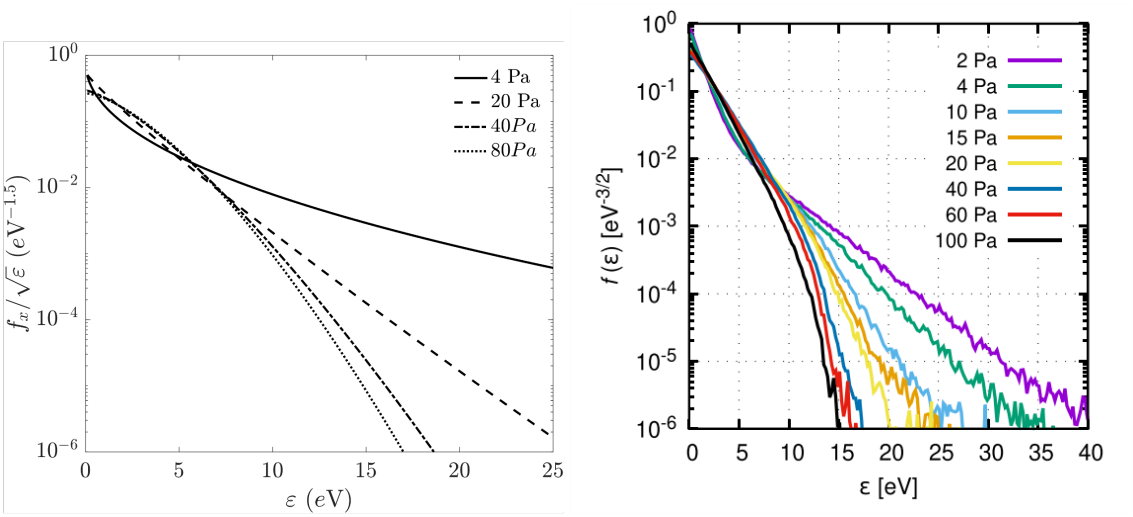

Fig. 6 (Left) The EEDFs obtained from the EnKF-CRM with OES data, reconstructed using the estimated α and T_e values. Reproduced from Ref. 3. (Right) The EEDFs obtained from a PIC-DRR model by Donko et al. Reproduced from Ref. 1.

Figure 6 shows that the EEDF estimated using the EnKF-CRM agrees well with the EEDFs obtained from a high-fidelity model by Donko et al. 1. The high-fidelity model uses a 1D particle-in-cell Monte Carlo collision (PIC-MCC) model that is coupled with a 1D diffusion reaction radiation (DRR) model. In the PIC-MCC model the ions and electrons with the number densities of ground state atoms that are obtained from the 1D DRR model. Overall, the agreement between the EnKF-CRM and the PIC-DRR model is good. At low pressure the high-energy tail is populated, while the EEDF becomes truncated at high energy for high pressure conditions. The EEDFs appear to be close to a Maxwellian distribution function around 15-20 Pa in both simulations.

B. EKF+PDE with LIF data

Here, the following predator-prey type model is considered

$$\frac{\partial n_i}{\partial t} + \frac{\partial}{\partial x}(n_i u_i) = n_i n_n k_{ion}(T_e) \tag{21}$$

$$\frac{\partial n_n}{\partial t} + \frac{\partial}{\partial x}(n_n u_n) = -n_i n_n k_{ion}(T_e) \tag{22}$$

where $n_i = n_i(x,t)$ is the ion density, $n_n = n_n(x,t)$ is the neutral atom density, $u_i = u_i(x,t)$ is the ion bulk velocity, u_n is the neutral atom bulk velocity that is assumed constant and uniform, k_ion is the ionization rate coefficient, and $T_e = T_e(x,t)$ is the electron temperature. The ionization rate coefficient is taken as a function of the electron temperature following Ref. 8. The set of the PDEs can be considered advection-reaction PDEs since the advection of both ions and neutrals are accounted for in addition to the ionization source/sink terms. The set of PDEs is the minimal set of equations that can generate a breathing mode type oscillation that is an ionization oscillation in the axial direction. As Hara et al. indicated the electron temperature fluctuation is required for an ionization instability in a zero-dimensional global model [9].

For the data assimilation, we use the spatio-temporal measurement data of ion bulk velocity from MacDonald-Tanenbaum et al. [2]. The discharge current oscillation is given in Fig. 7(a), where we accounted for a standard deviation of 20%. The discharge current oscillation helps anchor the ion density fluctuation, as we consider that the ion current at the channel exit is 80% of the discharge current. The ion VDFs are measured using LIF, i.e., u_i, is provided as a function of discrete time and spatial location. Similar to the EnKF-CRM study, the estimated measurement from the EKF shows good agreement with the discrete measurement data. For PDE estimation, we note that there is some uncertainty near the boundary, as can be seen in Fig. 7(c). This is due to the lack of experimental data near the boundary.

Figure 8 shows the spatio-temporal profiles of the ion density, neutral density, and electron temperature. It can be seen that the uncertainty of the ion density is largest in the discharge channel due to the lack of measurements as well as

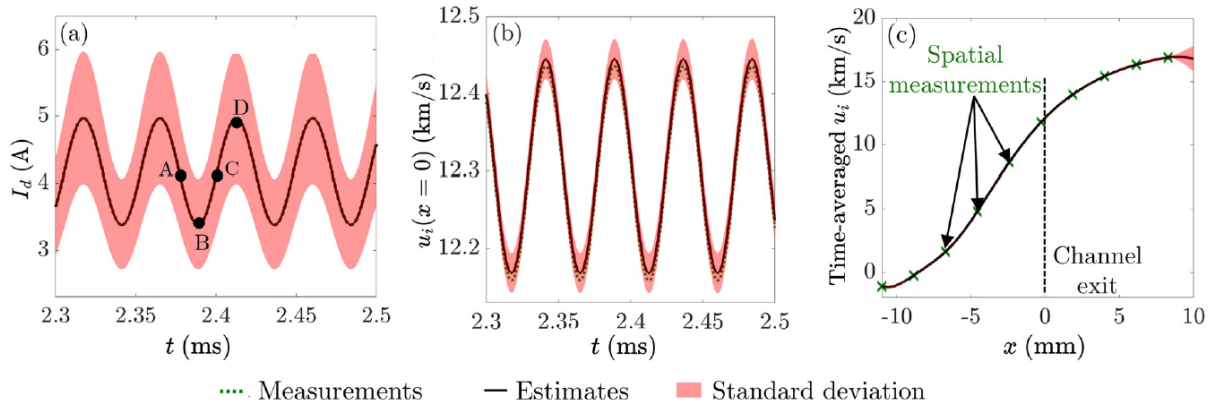

Fig. 7 Experimental data taken from Ref. 2. Reproduced from Ref. 3.

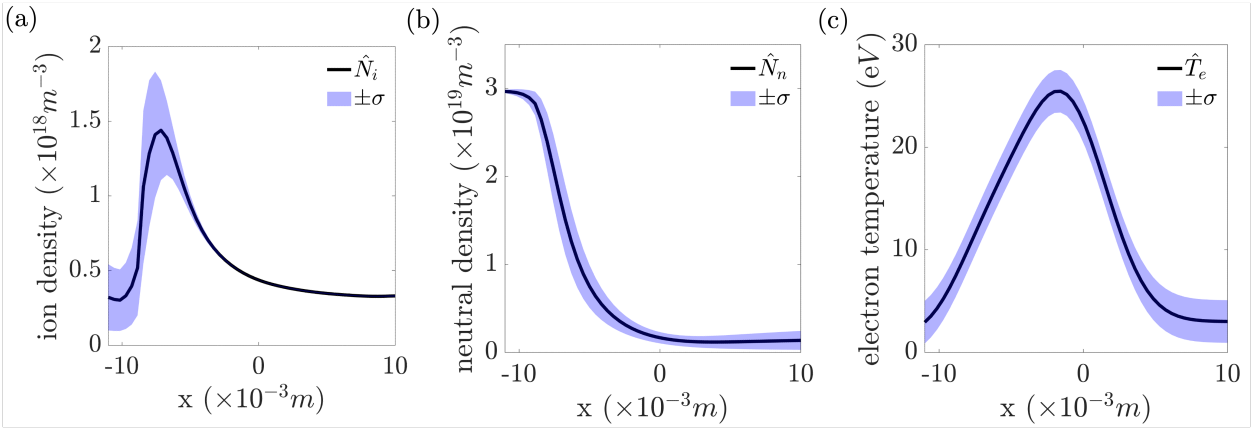

Fig. 8 Augmented state variables estimated in space at a given time.

due to the ionization oscillation. The neutral atom density shows an expected profile where the neutral density decreases in the ionization region. The electron temperature is treated as a parameter in this test case, without any dynamical model. Yet, the data assimilation shows that the electron temperature is estimated smoothly, primarily thanks to the spatial correlation noise.

IV. Conclusion

In this paper, we summarize the recent progress with state and parameter estimation of electron dynamics in plasma and electric propulsion applications. We present an EnKF coupled with CRM that is informed by OES data and an EKF coupled with a 1D PDE that is informed by LIF data. These methods highlight the usefulness of data assimilation for the electric propulsion applications.

Acknowledgments

This work was supported by NASA through the Joint Advanced Propulsion Institute, a NASA Space Technology Research Institute under Grant No. 80NSSC21K1118, the Air Force Office of Scientific Research under Award No. FA9550-21-1-0433, and Global Research Outreach program of Samsung Mechatronics Research.

References

[1] Donkó, Z., Tsankov, T. V., Hartmann, P., Arellano, F. J. T., Czarnetzki, U., and Hamaguchi, S., "Self-consistent calculation of the optical emission spectrum of an argon capacitively coupled plasma based on the coupling of particle simulation with a

collisional-radiative model," *J. Phys. D: Appl. Phys.*, 2024.

[2] MacDonald-Tenenbaum, N., Pratt, Q., Nakles, M., Pilgram, N., Holmes, M., and Hargus, W., "Background pressure effects on ion velocity distributions in an SPT-100 Hall thruster," *J. Propul. Power*, Vol. 35, No. 2, 2019, pp. 403–412.

[3] Dwivedi, A., and Hara, K., "Estimation of electron kinetics in low-temperature plasmas using data assimilation," *Journal of Physics D: Applied Physics*, Vol. 58, No. 17, 2025, p. 175203.

[4] Dwivedi, A., Cerepi, M., and Hara, K., "Spatiotemporal state and parameter estimation of plasma dynamics using data assimilation," *Physics of Plasmas*, Vol. 32, No. 6, 2025.

[5] Gudmundsson, J. T., "On the effect of the electron energy distribution on the plasma parameters of an argon discharge: a global (volume-averaged) model study," *Plasma Sources Sci. Technol.*, Vol. 10, No. 1, 2001, p. 76.

[6] Amemiya, H., "Sheath formation criterion and ion flux for non-Maxwellian plasma," *J. Phys. Soc. Jpn.*, Vol. 66, No. 5, 1997, pp. 1335–1338.

[7] Druyvesteyn, M. J., and Penning, F. M., "The mechanism of electrical discharges in gases of low pressure," *Rev. Mod. Phys.*, Vol. 12, No. 2, 1940, p. 87.

[8] Goebel, D. M., and Katz, I., *Ionization and Excitation Reaction Rates for Xenon in Maxwellian Plasmas*, 2008, pp. 475–477. https://doi.org/https://doi.org/10.1002/9780470436448.app5.

[9] Hara, K., Sekerak, M., Boyd, I., and Gallimore, A., "Perturbation analysis of ionization oscillations in Hall effect thrusters," *Phys. Plasmas*, Vol. 21, 2014, p. 122103. https://doi.org/10.1063/1.4903843.